Analysis of the radiative $\Lambda_b \to \Lambda\gamma$ transition in the standard model and scenarios with one or two universal extra dimensions

K. Azizi,[1,*] S. Kartal,[2,†] A. T. Olgun,[2,‡] and Z. Tavukoğlu[2,§]

[1]*Department of Physics, Doğuş University, Acıbadem-Kadıköy, 34722 İstanbul, Turkey*
[2]*Department of Physics, İstanbul University, Vezneciler, 34134 İstanbul, Turkey*

(Received 17 April 2013; published 26 July 2013)

We investigate the radiative process of $\Lambda_b \to \Lambda\gamma$ in the standard model as well as models with one or two compact universal extra dimensions. Using the form factors entered to the low-energy matrix elements, calculated via light-cone QCD in full theory, we calculate the total decay width and branching ratio of this decay channel. We compare the results of the extra-dimensional models with those of the standard model on the considered physical quantities and look for the deviations of the results from the standard model predictions at different values of the compactification scale $(1/R)$.

DOI: 10.1103/PhysRevD.88.015030 PACS numbers: 12.60.−i, 13.30.−a, 13.30.Ce, 14.20.Mr

I. INTRODUCTION

As it is well-known, the flavor-changing neutral current (FCNC) transitions are prominent tools to indirectly search for the new physics (NP) effects. There are many mesonic and baryonic processes based on the $b \to s$ transition at quark level investigated in the literature via different NP models and compared the obtained results with the experimental data to put constraints on the NP parameters. One of the most important channels in the agenda of different experimental groups is the baryonic FCNC $\Lambda_b \to \Lambda\ell^+\ell^-$ decay channel. The CDF Collaboration at Fermilab reported the first observation on this mode at the muon channel [1]. The measured branching ratio is comparable with the standard model (SM) prediction [2] within the errors of form factors. Comparing the different NP models' predictions with the experimental data on this channel, it is possible to obtain information about and put limits on the parameters of the models. In our previous work, we put a lower limit to the compactification parameter of the universal extra dimension (UED) via this channel, comparing the theoretical calculations with the experimental data [3].

The LHCb experiment at the LHC took data for proton-proton collision in 2011 and 2012 at $\sqrt{s} = 7$ and 8 TeV, respectively, integrating a luminosity in excess of 3 fb^{-1} [4,5]. The LHCb measurement on the differential branching ratio of the $\Lambda_b \to \Lambda\mu^+\mu^-$ is in its final stage [6]. Considering these experimental progresses and the accessed luminosity, we hope we will able to study more decay channels such as the radiative baryonic decay of $\Lambda_b \to \Lambda\gamma$ at LHCb [4–7]. In this connection, we study this radiative decay channel in the SM as well as a UED with a single extra dimension (UED5) and two extra dimensions (UED6) in the present work. There are many works dedicated to the analysis of different decay channels in the UED5 in the literature (for some of them, see Refs. [3,8–23]). However, the number of works devoted to the applications of the UED6 is relatively few. As the expression of the only Wilson coefficient C_7^{eff} now is available in the UED6 [24], it is possible to study the radiative channels based on the $b \to s\gamma$.

In Ref. [25], the UED6 is employed to analyze the $B \to K\eta^{(\prime)}\gamma$ decay channel, in which by comparing the results with the experimental data, a lower limit of 400 GeV is put for the compactification scale. For some other previous constraints on the compactification factor obtained via electroweak precision tests, some cosmological constraints, and different hadronic channels in the UED5, see, for instance, Refs. [3,11,26–30]. We shall use the latest lower limits on the compactification factor $1/R$ obtained from different FCNC transitions in the UED5 model [31], some FCNC transitions in the UED6 model [25], electroweak precision tests [29], cosmological constraints [32], direct searches [33], and the latest results of the Higgs search at the LHC and of the electroweak precision data for the S and T parameters [34].

Scenarios with extra dimensions (EDs) play crucial roles among models beyond the SM. The main feature that leads to the difference among ED models is the number of dimensions added to the SM. In the UED5, we have an extra universal compactified dimension compared to the SM, while in the UED6, we consider two extra UEDs. Because of the universality, the SM particles can propagate into the UEDs and interact with the Kaluza-Klein (KK) modes existing in EDs. As a result of these interactions, the new Feynman diagrams appear, and this leads to modifications in the Wilson coefficients entering the low-energy Hamiltonians defining the hadronic decay channels [10,24,35,36]. In the UED5, the ED is compactified to the orbifold S^1/Z_2, with the fifth coordinate $x_5 = y$ changing from 0 to $2\pi R$. The points $y = 0$ and $y = \pi R$ are fixed points of this orbifold. The boundary conditions at these points give the KK mode expansion of the fields.

*kazizi@dogus.edu.tr
†sehban@istanbul.edu.tr
‡a.t.olgun@gmail.com
§z.tavukoglu@gmail.com

 © 2013 American Physical Society

The masses of the KK particles in this model are obtained in terms of the compactification scale as $m_n{}^2 = m_0{}^2 + n^2/R^2$, where $n = 1, 2, \ldots$ and m_0 represents the zeroth mode mass referring to the SM particles (for more about the model, see Refs. [10,27,28,37–42]).

Models with two EDs are more attractive since they reply to some questions existing in the SM [43]. In this model, cancellations of chiral anomalies allow the existence of the right-handed neutrinos and predict the correct number of the fermion families [43–45]. At the same time, this model provides a natural explanation for the long lifetime of the proton [46,47]. In UED6 models also, all the SM fields are assumed to propagate into both flat EDs that are already compactified on a chiral square of the side $L = \pi R$ [24,43,48]. The KK particles existing in this model are marked by two positive integers k and l, which symbolize quantization of the momentum along the EDs. The masses of these particles are given in terms of the compactification scale by $M_{(k,l)} = \sqrt{k^2 + l^2}/R$ [43]. In this model, particles on first KK level with KK numbers (1, 0) are odd under KK parity. These particles may be produced only in pairs at colliders. The particles on level 2 are even under KK parity and have KK numbers (1, 1) [48]. This may lead to a totally different sets of signatures involving the resonances of the heavy top and bottom quarks [48,49]. The masses of particles on level 2 are a $\sqrt{2}$ factor larger than the masses of particles on level 1 [43]. This makes the particles at level 2 the most easily accessible at the LHC [49]. For more details about the UED6 model and some of its applications, see, for instance, Refs. [24,43,45–47,49].

The outline of the article is as follows. In next section, we present the effective Hamiltonian responsible for the $\Lambda_b \to \Lambda\gamma$ in the SM, UED5, and UED6 as well as the transition matrix elements in terms of form factors. In Sec. III, we calculate the decay width and branching ratio of the decay under consideration and numerically analyze them. In this section, we also compare the results of the UED5 and UED6 with the SM predictions and look for the deviations from the SM at different values of the compactification radius.

II. RADIATIVE $\Lambda_b \to \Lambda\gamma$ TRANSITION IN THE SM, UED5, AND UED6 MODELS

In the present section, we present the effective Hamiltonian and show how the Wilson coefficient $C_7^{\rm eff}$ changes in both UED scenarios with one and two extra dimensions compared to the SM. We also define the transition matrix elements appearing in the amplitude of the considered decay in terms of form factors.

A. Effective Hamiltonian

At the quark level, the general effective Hamiltonian for $b \to s\gamma$ and $b \to sg$ transitions in the SM and in terms of Wilson coefficients and operators is given by [35]

$$\mathcal{H}^{\rm eff} = -\frac{G_F}{\sqrt{2}} V_{tb} V_{ts}^* \Big[\sum_{i=1}^{6} C_i(\mu) Q_i(\mu) + C_{7\gamma}(\mu) Q_{7\gamma}(\mu) + C_{8G}(\mu) Q_{8G}(\mu) \Big], \tag{2.1}$$

where G_F is the Fermi weak coupling constant and V_{ij} are elements of the Cabibbo-Kobayashi-Maskawa mixing matrix. The complete list of the operators entered to the above Hamiltonian is given as

$$\begin{aligned}
Q_1 &= (\bar{s}_\alpha c_\beta)_{V-A} (\bar{c}_\beta b_\alpha)_{V-A}, \\
Q_2 &= (\bar{s}_\alpha c_\alpha)_{V-A} (\bar{c}_\beta b_\beta)_{V-A}, \\
Q_3 &= (\bar{s}_\alpha b_\alpha)_{V-A} \sum_q (\bar{q}_\beta q_\beta)_{V-A}, \\
Q_4 &= (\bar{s}_\beta b_\alpha)_{V-A} \sum_q (\bar{q}_\alpha q_\beta)_{V-A}, \\
Q_5 &= (\bar{s}_\alpha b_\alpha)_{V-A} \sum_q (\bar{q}_\beta q_\beta)_{V+A}, \\
Q_6 &= (\bar{s}_\beta b_\alpha)_{V-A} \sum_q (\bar{q}_\alpha q_\beta)_{V+A}, \\
Q_{7\gamma} &= \frac{e}{4\pi^2} \bar{s}_\alpha \sigma^{\mu\nu} (m_b R + m_s L) b_\alpha F_{\mu\nu}, \\
Q_{8G} &= \frac{g_s}{4\pi^2} \bar{s}_\alpha \sigma^{\mu\nu} (m_b R + m_s L) T^a_{\alpha\beta} b_\beta G^a_{\mu\nu},
\end{aligned} \tag{2.2}$$

where $Q_{1,2}$, $Q_{3,4,5,6}$, and $Q_{7\gamma,8G}$ are the current-current (tree), QCD penguin, and the magnetic penguin operators, respectively. α and β are the color indices, $R = (1 + \gamma_5)/2$ is the right-handed projector, and $L = (1 - \gamma_5)/2$ is the left-handed projector. In the above operators, e and g_s are the coupling constants of the electromagnetic and strong interactions, respectively. $F_{\mu\nu}$ is the field strength tensor of the electromagnetic field and is defined by

$$F_{\mu\nu}(x) = -i(\varepsilon_\mu q_\nu - \varepsilon_\nu q_\mu) e^{iqx}, \tag{2.3}$$

where ε_μ is the polarization vector of the photon and q is its momentum. The most relevant contribution to $b \to s\gamma$ comes from the magnetic penguin operator $Q_{7\gamma}$. Hence, the effective Hamiltonian in our case can be written as

$$\mathcal{H}^{\rm eff}(b \to s\gamma) = -\frac{G_F e}{4\pi^2\sqrt{2}} V_{tb} V_{ts}^* C_7^{\rm eff}(\mu) \bar{s} \times \sigma_{\mu\nu} [m_b R + m_s L] b F^{\mu\nu}, \tag{2.4}$$

where $C_7^{\rm eff}$ is relevant the Wilson coefficient. Under scenarios with EDs including one or two compact extra dimensions, the form of the effective Hamiltonian remains unchanged, but the Wilson coefficient $C_7^{\rm eff}$ is modified because of additional Feynman diagrams coming from the interactions of the KK particles with themselves as well as the SM particles in the bulk. This coefficient in the SM is given as [50]

$$C_7^{\rm eff}(\mu_b) = \eta^{\frac{16}{23}} C_7(\mu_W) + \frac{8}{3}(\eta^{\frac{14}{23}} - \eta^{\frac{16}{23}}) C_8(\mu_W) + C_2(\mu_W) \sum_{i=1}^{8} h_i \eta^{a_i}, \tag{2.5}$$

where

$$\eta = \frac{\alpha_s(\mu_W)}{\alpha_s(\mu_b)}, \tag{2.6}$$

and

$$\alpha_s(x) = \frac{\alpha_s(m_Z)}{1 - \beta_0 \frac{\alpha_s(m_Z)}{2\pi} \ln\left(\frac{m_Z}{x}\right)}. \tag{2.7}$$

Here, $\alpha_s(m_Z) = 0.118$ and $\beta_0 = \frac{23}{3}$. The values of coefficients a_i and h_i in Eq. (2.5) are given as

$$\begin{aligned} a_i &= \left(\frac{14}{23}, \frac{16}{23}, \frac{6}{23}, -\frac{12}{23}, 0.4086, -0.4230, -0.8994, 0.1456\right), \\ h_i &= \left(2.2996, -1.0880, -\frac{3}{7}, -\frac{1}{11}, -0.6494, 0.0380, -0.0186, -0.0057\right). \end{aligned} \tag{2.8}$$

Also, $C_2(\mu_W)$, $C_7(\mu_W)$, and $C_8(\mu_W)$ in Eq. (2.5) are defined in the following way:

$$C_2(\mu_W) = 1, \qquad C_7(\mu_W) = -\frac{1}{2} D_0'(x_t), \qquad C_8(\mu_W) = -\frac{1}{2} E_0'(x_t), \tag{2.9}$$

where $D_0'(x_t)$ and $E_0'(x_t)$ are expressed as

$$D_0'(x_t) = -\frac{(8x_t^3 + 5x_t^2 - 7x_t)}{12(1-x_t)^3} + \frac{x_t^2(2-3x_t)}{2(1-x_t)^4} \ln x_t, \tag{2.10}$$

$$E_0'(x_t) = -\frac{x_t(x_t^2 - 5x_t - 2)}{4(1-x_t)^3} + \frac{3x_t^2}{2(1-x_t)^4} \ln x_t. \tag{2.11}$$

The Wilson coefficient $C_7^{\rm eff}$ in the UED5 has been calculated in Refs. [9,10,35,50–52]. In this model, each periodic function $F(x_t, 1/R)$ ($F = D'$ or E') inside the Wilson coefficient includes a SM part $F_0(x_t)$ plus an additional part in terms of compactification factor $1/R$ due to new interactions, i.e.,

$$F(x_t, 1/R) = F_0(x_t) + \sum_{n=1}^{\infty} F_n(x_t, x_n), \tag{2.12}$$

where $x_t = \frac{m_t^2}{m_W^2}$, $x_n = \frac{m_n^2}{m_W^2}$, and $m_n = \frac{n}{R}$. Here, m_t, m_W, and m_n are masses of the top quark, W boson, and KK particles (nonzero modes), respectively. In the UED5, the functions $D'(x_t, 1/R)$ and $E'(x_t, 1/R)$ in terms of compactification parameter $1/R$ are given as

$$\begin{aligned} D'(x_t, 1/R) &= D_0'(x_t) + \sum_{n=1}^{\infty} D_n'(x_t, x_n), \\ E'(x_t, 1/R) &= E_0'(x_t) + \sum_{n=1}^{\infty} E_n'(x_t, x_n), \end{aligned} \tag{2.13}$$

where the functions including KK contributions are written as

$$\begin{aligned} \sum_{n=1}^{\infty} D_n'(x_t, x_n) = {} & \frac{x_t[37 - x_t(44 + 17x_t)]}{72(x_t - 1)^3} + \frac{\pi m_W R}{12}\Bigg[\int_0^1 dy(2y^{1/2} + 7y^{3/2} + 3y^{5/2}) \coth(\pi m_W R\sqrt{y}) \\ & - \frac{x_t(2 - 3x_t)(1 + 3x_t)}{(x_t - 1)^4} J(R, -1/2) - \frac{1}{(x_t - 1)^4}\{x_t(1 + 3x_t) + (2 - 3x_t)[1 - (10 - x_t)x_t]\} J(R, 1/2) \\ & - \frac{1}{(x_t - 1)^4}[(2 - 3x_t)(3 + x_t) + 1 - (10 - x_t)x_t] J(R, 3/2) - \frac{(3 + x_t)}{(x_t - 1)^4} J(R, 5/2)\Bigg], \end{aligned} \tag{2.14}$$

and

$$\begin{aligned} \sum_{n=1}^{\infty} E_n'(x_t, x_n) = {} & \frac{x_t[17 + (8 - x_t)x_t]}{24(x_t - 1)^3} + \frac{\pi m_W R}{4}\Bigg[\int_0^1 dy(y^{1/2} + 2y^{3/2} - 3y^{5/2}) \coth(\pi m_W R\sqrt{y}) - \frac{x_t(1 + 3x_t)}{(x_t - 1)^4} J(R, -1/2) \\ & + \frac{1}{(x_t - 1)^4}[x_t(1 + 3x_t) - 1 + (10 - x_t)x_t] J(R, 1/2) - \frac{1}{(x_t - 1)^4}[(3 + x_t) - 1 + (10 - x_t)x_t] J(R, 3/2) \\ & + \frac{(3 + x_t)}{(x_t - 1)^4} J(R, 5/2)\Bigg], \end{aligned} \tag{2.15}$$

where

$$J(R, \alpha) = \int_0^1 dy y^{\alpha}[\coth(\pi m_W R\sqrt{y}) - x_t^{1+\alpha} \coth(\pi m_t R\sqrt{y})]. \tag{2.16}$$

The Wilson coefficient $C_7^{\rm eff}(1/R)$ in the UED6 model with two extra dimensions is given by [24]

$$C_i^{\rm eff}(\mu) = C_{i\rm SM}^{\rm eff}(\mu) + \Delta C_i^{\rm eff}(\mu), \quad i = 1, \ldots, 8, \tag{2.17}$$

where

$$\Delta C_i^{\rm eff}(\mu) = \sum_{n=0}^{\infty} \left(\frac{\alpha_s}{4\pi}\right)^n \Delta C_i^{{\rm eff}(n)}(\mu), \tag{2.18}$$

and

$$\Delta C_i^{{\rm eff}(0)}(\mu_0) = \begin{cases} 0 & \text{for } i = 1, \ldots, 6, \\ -\frac{1}{2}\sum_{k,l}' A^{(0)}(x_{kl}) & \text{for } i = 7, \\ -\frac{1}{2}\sum_{k,l}' F^{(0)} & \text{for } i = 8. \end{cases} \tag{2.19}$$

The superscript $\prime$ in summation means that the KK sums run only over the restricted ranges $k \geq 1$ and $l \geq 0$, i.e., $\sum_{k,l}' = \sum_{k\geq 1}\sum_{l\geq 0}$. The upper limits for k and l are restricted as $k + l \leq N_{\rm KK}$, where $N_{\rm KK}$ can get values in the interval (5–15) [24]. The parameter $N_{\rm KK}$ in our calculations is the total number of contributing KK modes [28]. The highest KK level in this compactification is fixed by $N_{\rm KK} = \Lambda R$ [53], where Λ is a scale at which the QCD interactions become strong in the ultraviolet [49]. In the case of UED5 $N_{\rm KK} = n$, however, as the KK summing over n up to infinity is convergent, we have no dependence on the $N_{\rm KK}$ after the KK sums. In the case of UED6, the KK mode sums diverge in the limit $N_{\rm KK} \to \infty$ because the KK spectrum is denser than the UED5 case. The electroweak observables convergence in four and five dimensions at one loop become logarithmically divergent at $d = 6$ and more divergent in higher dimensions [28]. Hence, we should put a cutoff and, as a result, an upper limit to $k + l$.

The Inami-Lim functions inside the $C_7^{\rm eff}$ in leading order are decomposed as

$$X^{(0)}(x_{kl}) = \sum_{I=W,a,H} X_I^{(0)}(x_{kl}), \qquad X = A, F, \tag{2.20}$$

where x_{kl} is defined as

$$x_{kl} = (k^2 + l^2)/(R^2 m_W^2), \tag{2.21}$$

and the functions $X_{W,a,H}^{(0)}(x_{kl})$ define the contributions because of the exchange of KK modes, which would be the Goldstone bosons $G_{(kl)}^{\pm}$, W-bosons $W_{\mu(kl)}^{\pm}$, and the scalar fields $a_{(kl)}^{\pm}$ as well as $W_{H(kl)}^{\pm}$. They are given as

$$A_W^{(0)}(x_{kl}) = \frac{x_t(6((x_t-3)x_t+3)x_{kl}^2 - 3(5(x_t-3)x_t+6)x_{kl} + x_t(8x_t+5) - 7)}{12(x_t-1)^3} + \frac{1}{2}(x_{kl}-2)x_{kl}^2 \ln\left(\frac{x_{kl}}{x_{kl}+1}\right) - \frac{(x_{kl}+x_t)^2(x_{kl}+3x_t-2)}{2(x_t-1)^4}\ln\left(\frac{x_{kl}+x_t}{x_{kl}+1}\right), \tag{2.22}$$

$$F_W^{(0)}(x_{kl}) = \frac{x_t(-6((x_t-3)x_t+3)x_{kl}^2 - 3((x_t-3)x_t+6)x_{kl} + (x_t-5)x_t - 2)}{4(x_t-1)^3} - \frac{3}{2}(x_{kl}+1)x_{kl}^2 \ln\left(\frac{x_{kl}}{x_{kl}+1}\right) + \frac{3(x_{kl}+1)(x_{kl}+x_t)^2}{2(x_t-1)^4}\ln\left(\frac{x_{kl}+x_t}{x_{kl}+1}\right), \tag{2.23}$$

$$A_a^{(0)}(x_{kl}) = \frac{x_t(6x_{kl}^2 - 3(x_t(2x_t-9)+3)x_{kl} + (29-7x_t)x_t - 16)}{36(x_t-1)^3} - \frac{(x_{kl}+3x_t-2)(x_t + x_{kl}((x_{kl}-x_t+4)x_t-1))}{6(x_t-1)^4} \times \ln\left(\frac{x_{kl}+x_t}{x_{kl}+1}\right) - \frac{1}{6}(x_{kl}-2)x_{kl}\ln\left(\frac{x_{kl}}{x_{kl}+1}\right), \tag{2.24}$$

$$F_a^{(0)}(x_{kl}) = \frac{x_t(-6x_{kl}^2 + (6x_t^2 - 9x_t - 9)x_{kl} + (7-2x_t)x_t - 11)}{12(x_t-1)^3} + \frac{(x_{kl}+1)(x_t + x_{kl}((x_{kl}-x_t+4)x_t-1))}{2(x_t-1)^4}\ln\left(\frac{x_{kl}+x_t}{x_{kl}+1}\right) + \frac{1}{2}x_{kl}(x_{kl}+1)\ln\left(\frac{x_{kl}}{x_{kl}+1}\right), \tag{2.25}$$

$$A_H^{(0)}(x_{kl}) = \frac{x_t(6(x_t^2-3x_t+3)x_{kl}^2 - 3(3x_t^2-9x_t+2)x_{kl} - 7x_t^2 + 29x_t - 16)}{36(x_t-1)^3} - \frac{(x_{kl}+1)(x_{kl}^2 + (4x_t-2)x_{kl} + x_t(3x_t-2))}{6(x_t-1)^4}\ln\left(\frac{x_{kl}+x_t}{x_{kl}+1}\right) + \frac{1}{6}x_{kl}(x_{kl}^2 - x_{kl} - 2)\ln\left(\frac{x_{kl}}{x_{kl}+1}\right), \tag{2.26}$$

and

$$F_H^{(0)}(x_{kl}) = -\frac{x_t(6(x_t^2-3x_t+3)x_{kl}^2+3(3x_t^2-9x_t+10)x_{kl}+2x_t^2-7x_t+11)}{12(x_t-1)^3} - \frac{1}{2}x_{kl}(x_{kl}+1)^2\ln\left(\frac{x_{kl}}{x_{kl}+1}\right) + \frac{(x_{kl}+x_t)(x_{kl}+1)^2}{2(x_t-1)^4}\ln\left(\frac{x_{kl}+x_t}{x_{kl}+1}\right). \quad (2.27)$$

B. Transition amplitude and matrix elements

The amplitude for this transition is obtained by sandwiching the effective Hamiltonian between the final and initial baryonic states,

$$\mathcal{M}^{(\Lambda_b\to\Lambda\gamma)} = \langle\Lambda(p_\Lambda)|\mathcal{H}^{\rm eff}|\Lambda_b(p_{\Lambda_b})\rangle, \quad (2.28)$$

where p_Λ and p_{Λ_b} are momenta of the Λ and Λ_b baryons, respectively. In order to proceed, we need to define the following transition matrix elements in terms of two form factors f_2^T and g_2^T:

$$\langle\Lambda(p_\Lambda)|\bar{s}\sigma_{\mu\nu}q^\nu(g_V+\gamma_5 g_A)b|\Lambda_b(p_{\Lambda_b})\rangle = \bar{u}_\Lambda(p_\Lambda)\sigma_{\mu\nu}q^\nu(g_V f_2^T(0)+\gamma_5 g_A g_2^T(0))u_{\Lambda_b}(p_{\Lambda_b}), \quad (2.29)$$

where $g_V = 1+m_s/m_b$, $g_A = 1-m_s/m_b$, and $\bar{u}_\Lambda$ and u_{Λ_b} are spinors of the Λ and Λ_b baryons, respectively. In the following, we will use the values of the form factors calculated via light-cone QCD sum rules in full theory [2].

III. DECAY WIDTH AND BRANCHING RATIO

In this section, we would like to calculate the total decay width and branching ratio of the transition under consideration. Using the aforementioned transition matrix elements in terms of form factors, we find the $1/R$-dependent total decay width in terms of the two form factors as

$$\Gamma_{(\Lambda_b\to\Lambda\gamma)}(1/R) = \frac{G_F^2\alpha_{\rm em}|V_{tb}V_{ts}^*|^2 m_b^2}{64\pi^4} \times |C_7^{\rm eff}(1/R)|^2\left(\frac{m_{\Lambda_b}^2-m_\Lambda^2}{m_{\Lambda_b}}\right)^3 \times (g_V^2|f_2^T(0)|^2+g_A^2|g_2^T(0)|^2), \quad (3.1)$$

where $\alpha_{\rm em}$ is the fine structure constant at the Z mass scale. In order to calculate the $1/R$-dependent branching ratio, we need to multiply the total decay width by the lifetime of the initial baryon Λ_b and divide by $\hbar$. To numerically analyze the obtained results, we use some input parameters as presented in Table I. For the quark masses, we use the $\overline{\rm MS}$ scheme values [54] (see Table II).

As we previously mentioned, we use the values of form factors calculated via light-cone QCD sum rules in full theory as the main inputs in numerical analysis [2]. Their values are presented in Table III.

In this part, we present the numerical values of the Wilson coefficient $C_7^{\rm eff}$ obtained from the previously presented formulas in the SM, UED5, and UED6 models. In the SM, its value is obtained as $C_7^{\rm eff} = -0.295$. We depict the values of the Wilson coefficient $C_7^{\rm eff}$ at different values of $1/R$ in the UED5 and UED6 scenarios with $N_{\rm KK} = (5, 10, 15)$ in Table IV.

Making use of all given input values, we find the value of the branching ratio in the SM as presented in Table V. For comparison, we also give the results of other related works [55–60] in the same table as well as the upper limit from the Particle Data Group (PDG)[54]. From this table we see that, within the errors, our result is consistent with those of QCD sum rules [56,57] and a special current [59] and exactly the same with pole model's prediction [60]. However, our prediction differs considerably from these of light-cone QCD sum rules [55], covariant oscillator quark model (COQM) [58] and Ioffe current [59]. The

TABLE I. The values of some input parameters, mainly taken from the Particle Data Group [54], used in the numerical analysis.

Input parameters	Values
m_W	80.38 GeV
m_{Λ_b}	5.619 GeV
m_Λ	1.1156 GeV
μ_b	5 GeV
μ_W	80.4 GeV
μ_0	160 GeV
τ_{Λ_b}	1.425×10^{-12} s
$\hbar$	6.582×10^{-25} GeV s
G_F	1.17×10^{-5} GeV^{-2}
$\alpha_{\rm em}$	1/137
$\lvert V_{tb}V_{ts}^*\rvert$	0.041

TABLE II. The values of quark masses in the $\overline{\rm MS}$ scheme [54].

Quarks	Masses in $\overline{\rm MS}$ scheme
m_s	(0.095 ± 0.005) GeV
m_b	(4.18 ± 0.03) GeV
m_t	$160^{+4.8}_{-4.3}$ GeV

TABLE III. The values of form factors $f_2^T(0)$ and $g_2^T(0)$ [2].

Form factors at $q^2=0$	
$f_2^T(0)$	0.295 ± 0.105
$g_2^T(0)$	0.294 ± 0.105

TABLE IV. The numerical values of Wilson coefficient $C_7^{\rm eff}$ at the different values of $1/R$ in the UED5 and UED6 for $N_{\rm KK} = (5, 10, 15)$.

$1/R$ [GeV]	$C_7^{\rm eff}$ (UED5)	$C_7^{\rm eff}$ (UED6 for $N_{\rm KK} = 5$)	$C_7^{\rm eff}$ (UED6 for $N_{\rm KK} = 10$)	$C_7^{\rm eff}$ (UED6 for $N_{\rm KK} = 15$)
200	−0.198	−0.053	0.048	0.110
400	−0.265	−0.224	−0.198	−0.182
600	−0.281	−0.262	−0.250	−0.243
800	−0.287	−0.276	−0.269	−0.265
1000	−0.289	−0.283	−0.278	−0.279

TABLE V. The values of branching ratio in SM.

Reference	BR($\Lambda_b \to \Lambda\gamma$)
Our result	$(1.003 - 4.457) \times 10^{-5}$
Light-cone sum rule [55]	$(0.63 - 0.73) \times 10^{-5}$
Three-point QCD sum rule [56]	$(3.1 \pm 0.6) \times 10^{-5}$
QCD sum rule [57]	$(3.7 \pm 0.5) \times 10^{-5}$
COQM [58]	0.23×10^{-5}
Special current [59]	$(1.99^{+0.34}_{-0.31}) \times 10^{-5}$
Ioffe current [59]	$(0.61^{+0.14}_{-0.13}) \times 10^{-6}$
Pole model [60]	$(1.0 - 4.5) \times 10^{-5}$
PDG [54]	$<1.3 \times 10^{-3}$ $(CL = 90\%)$

difference between our SM prediction on the branching ratio with that of Ref. [55] with the same method can be attributed to the point that in Ref. [55] the authors consider the distribution amplitudes (DAs) of an Λ baryon as the main inputs of the light-cone QCD sum rule method up to twist 6; however, in our case, the form factors have been calculated considering the DAs up to twist 8. Besides, in Ref. [55] the higher conformal spin contributions to the DAs are not taken into account, while the calculations of form factors in our case include these contributions. Finally, in Ref. [55] the form factors are calculated in the heavy quark effective limit while we use form factors calculated in full QCD without any approximation. The order of the branching ratio shows that this channel can be accessible at the LHCb.

In order to look for the differences between the predictions of the SM and the considered UED scenarios, we present the dependence of the central values of the branching ratio on $1/R$ at different models in Fig. 1. Note that to better see the deviations between the SM predictions and those of UED scenarios, in all figures, we plot the branching ratio in terms of $1/R$ in the interval 200 GeV $\leq 1/R \leq$ 2000 GeV. However, we will consider the latest lower limits on the compactification factor obtained from different approaches in our analysis and discussions. The latest lower limits on $1/R$ are 400 GeV put by some FCNC transitions in the UED6 model [25], 500 GeV put via cosmological constraints [32], 600 GeV obtained via different FCNC transitions in the UED5 model (for instance, see Ref. [31]) and electroweak precision tests [29], and 1.41 TeV quoted via direct searches at the ATLAS Collaboration [33], as well as 650(850 ∼ 1350) GeV from the latest results of the Higgs search/discovery at the LHC for the UED5 (UED6) [34] and 700(900 ∼ 1500) GeV from the electroweak precision data for S and T parameters in the case of the UED5 (UED6) [34].

From Fig. 1, we see that there are distinctive differences between the SM predictions and those of the UED models, especially the UED6 for $N_{\rm KK} = 15$, at small values of the

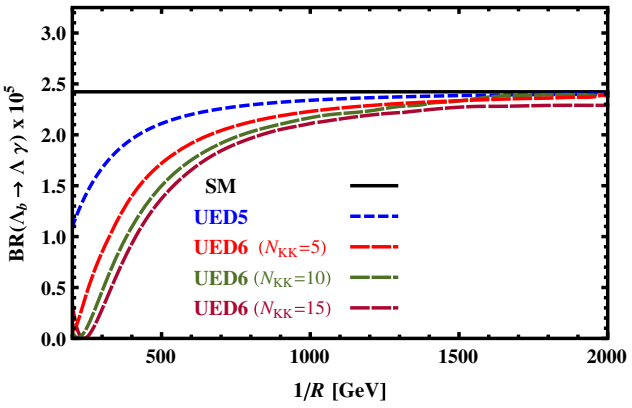

FIG. 1 (color online). The dependence of the branching ratio for the $\Lambda_b \to \Lambda\gamma$ decay channel on compactification factor $1/R$ in the SM, UED5, and UED6 models with $N_{\rm KK} = (5, 10, 15)$ when the central values of the form factors are used.

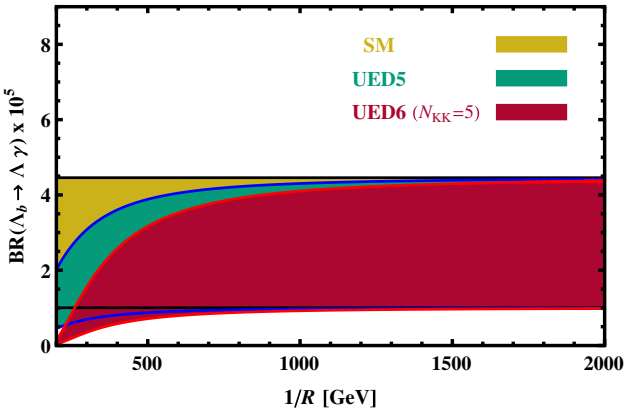

FIG. 2 (color online). The dependence of the branching ratio on compactification factor $1/R$ for $\Lambda_b \to \Lambda\gamma$ decay in the SM, UED5, and UED6 with $N_{\rm KK} = 5$ when the uncertainties of the form factors are considered.

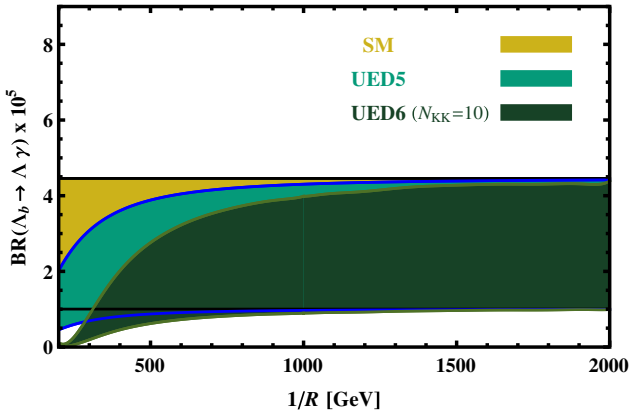

FIG. 3 (color online). The same as Fig. 2 but for $N_{\rm KK} = 10$.

compactification factor $1/R$. These differences exist in the lower limits obtained by different FCNC transitions in the UED5 and UED6, cosmological constraints, electroweak precision tests [25,29,31,32], and the latest results of the Higgs search at the LHC and of the electroweak precision data for the S and T parameters [34]; however, they become small when $1/R$ approaches 1 TeV. Our analysis show that the UED scenarios give close results to the SM for $1/R \geq 1$ TeV. Hence, when considering the lower limit 1.41 TeV quoted via direct searches at the ATLAS Collaboration [33], we see very small deviations of the UED model predictions from those of the SM for the decay channel under consideration.

At the end of this section, we present the dependence of the branching ratio on $1/R$ considering the errors of form factors in Figs. 2–4. From these figures, we read that the errors of form factors cannot totally kill the differences between the predictions of the UED models on the branching ratio of the $\Lambda_b \to \Lambda\gamma$ channel with that of the SM at lower values of the compactification scale. These discrepancies can also be seen in the lower limits favored by different FCNC transitions in the UED5 and UED6 models, cosmological constraints, and electroweak precision tests [25,29,31,32], as well as the latest results of the Higgs search/discovery at the LHC and of the electroweak precision data for the S and T parameters [34] for the UED5. However, when $1/R$ approaches 1 TeV all differences of the UED results with the SM predictions are roughly killed, and there are no considerable deviations of the UED predictions from that of the SM at 1.41 TeV quoted via direct searches at the ATLAS Collaboration [33] for the $\Lambda_b \to \Lambda\gamma$ decay channel.

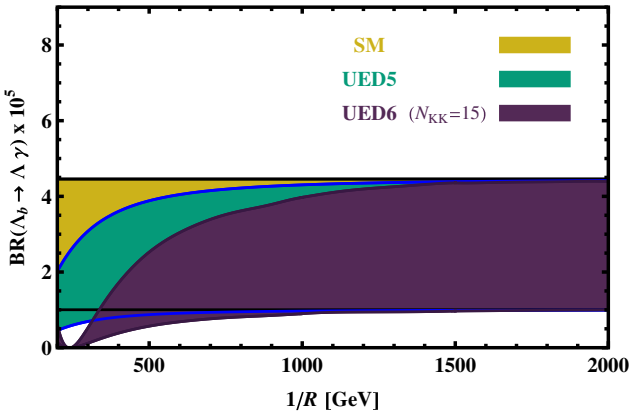

FIG. 4 (color online). The same as Fig. 2 but for $N_{\rm KK} = 15$.

IV. CONCLUSION

In the present work, we have performed a comprehensive analysis of the $\Lambda_b \to \Lambda\gamma$ decay channel in the SM, UED5, and UED6 scenarios. In particular, we calculated the total decay rate and branching ratio for this channel in different UED scenarios and looked for the deviations of the results from the SM predictions. We used the expression of the Wilson coefficient $C_7^{\rm eff}$ entering the low-energy effective Hamiltonian calculated in the SM, UED5, and UED6 models. We also used the numerical values of the form factors calculated via light-cone QCD sum rules in full theory as the main inputs of the numerical analysis. We detected considerable discrepancies between the considered UED models' predictions with that of the SM prediction at lower values of the compactification factor. These discrepancies cannot totally be killed by the uncertainties of the form factors at lower values of $1/R$, and they exist at the lower limits favored by different FCNC transitions in the UED5 and UED6 models, cosmological constraints, and electroweak precision tests [25,29,31,32], as well as the latest results of the Higgs search/discovery at the LHC and of the electroweak precision data for the S and T parameters [34]. However, when $1/R$ approaches 1 TeV all deviations of the UED results from the SM predictions are roughly killed, and there are no considerable deviations of the UED predictions for the $\Lambda_b \to \Lambda\gamma$ decay channel from that of the SM at 1.41 TeV quoted via direct searches at the ATLAS Collaboration [33]. The order of the branching ratio for the $\Lambda_b \to \Lambda\gamma$ decay channel in the SM shows that this channel can be accessible at the LHCb.

ACKNOWLEDGMENTS

We would like to thank A. Freitas and U. Haisch for useful discussions.

Note added.—After completing this work, a related study titled "Bounds on the compactification scale of two universal extra dimensions from exclusive $b \to s\gamma$ decays" was submitted to the e-print archives on February 28, 2013, as [61], in which a similar analysis is done only in the UED6 using the form factors calculated from the heavy quark effective theory and average value of the $N_{\rm KK}$. When we compare our results with those of Ref. [61], we see that there is a considerable difference between our result on the branching ratio of the decay

under consideration in the SM with those of Ref. [61]. Although the central values of the branching ratios in the two works obtained via the UED6 have similar behaviors, the bands of the UED6 in our case sweep wide ranges compared to those of Ref. [61]. Especially, the band of the UED6 ($N_{\rm KK} = 10$) in Ref. [61] starts to completely cover the SM band at $1/R \approx 800$ GeV, while in our case, we see a similar behavior at $1/R \approx 1000$ GeV. These small differences can be attributed to different form factors used in the numerical analysis as well as other input parameters.

[1] T. Aaltonen *et al.* (CDF Collaboration), Phys. Rev. Lett. **107**, 201802 (2011).
[2] T. M. Aliev, K. Azizi, and M. Savci, Phys. Rev. D **81**, 056006 (2010).
[3] K. Azizi, S. Kartal, N. Katirci, A. T. Olgun, and Z. Tavukoglu, J. High Energy Phys. 05 (2012) 024.
[4] C. Bozzi, arXiv:1303.4219.
[5] M.-H. Schune (LHCb Collaboration), Report No. LHCB-PROC 005, 2013 (unpublished).
[6] M. Kreps (private communication).
[7] G. Mancinelli, in Proceedings of Recontres du Vietnam, Beyond the Standard Model of Particle Physics, Qui Nhon, Vietnam, 2012 (unpublished).
[8] K. Azizi and N. Katirci, J. High Energy Phys. 01 (2011) 087.
[9] A. J. Buras, M. Spranger, and A. Weiler, Nucl. Phys. **B660**, 225 (2003).
[10] A. J. Buras, A. Poschenrieder, M. Spranger, and A. Weiler, Nucl. Phys. **B678**, 455 (2004).
[11] P. Colangelo, F. De Fazio, R. Ferrandes, and T. N. Pham, Phys. Rev. D **73**, 115006 (2006).
[12] V. Bashiry and K. Azizi, J. High Energy Phys. 02 (2012) 021.
[13] N. Katirci and K. Azizi, J. High Energy Phys. 07 (2011) 043.
[14] V. Bashiry, M. Bayar, and K. Azizi, Phys. Rev. D **78**, 035010 (2008).
[15] Y.-M. Wang, M. J. Aslam, and C.-D. Lü, Eur. Phys. J. C **59**, 847 (2009).
[16] T. M. Aliev and M. Savcı, Eur. Phys. J. C **50**, 91 (2007).
[17] F. De Fazio, Nucl. Phys. B, Proc. Suppl. **174**, 185 (2007).
[18] B. B. Sirvanli, K. Azizi, and Y. Ipekoglu, J. High Energy Phys. 01 (2011) 069.
[19] K. Azizi, N. K. Pak, and B. B. Sirvanli, J. High Energy Phys. 02 (2012) 034.
[20] T. M. Aliev, M. Savci, and B. B. Sirvanli, Eur. Phys. J. C **52**, 375 (2007).
[21] I. Ahmed, M. A. Paracha, and M. J. Aslam, Eur. Phys. J. C **54**, 591 (2008).
[22] P. Colangelo, F. De Fazio, R. Ferrandes, and T. N. Pham, Phys. Rev. D **74**, 115006 (2006).
[23] R. Mohanta and A. K. Giri, Phys. Rev. D **75**, 035008 (2007).
[24] A. Freitas and U. Haisch, Phys. Rev. D **77**, 093008 (2008).
[25] P. Biancofiore, P. Colangelo, and F. D. Fazio, Phys. Rev. D **85**, 094012 (2012).
[26] J. A. R. Cembranos, J. L. Feng, and L. E. Strigari, Phys. Rev. D **75**, 036004 (2007).
[27] T. Appelquist and H.-U. Yee, Phys. Rev. D **67**, 055002 (2003).
[28] T. Appelquist, H. C. Cheng, and B. A. Dobrescu, Phys. Rev. D **64**, 035002 (2001).
[29] I. Gogoladze and C. Macesanu, Phys. Rev. D **74**, 093012 (2006).
[30] K. Agashe, N. G. Deshpande, and G.-H. Wu, Phys. Lett. B **514**, 309 (2001).
[31] U. Haisch and A. Weiler, Phys. Rev. D **76**, 034014 (2007).
[32] G. Belanger, M. Kakizaki, and A. Pukhov, J. Cosmol. Astropart. Phys. 02 (2011) 009.
[33] ATLAS Collaboration, Report No. ATLAS-CONF-2012-072, 2012.
[34] T. Kakuda, K. Nishiwaki, K.-y. Oda, N. Okuda, and R. Watanabe, arXiv:1304.6362; T. Kakuda, K. Nishiwaki, K.-y. Oda, and R. Watanabe, arXiv:1305.1686.
[35] G. Buchalla, A. J. Buras, and M. E. Lautenbacher, Rev. Mod. Phys. **68**, 1125 (1996).
[36] A. J. Buras, L. Merlo, and E. Stamou, J. High Energy Phys. 08 (2011) 124.
[37] I. Antoniadis, Phys. Lett. B **246**, 377 (1990).
[38] I. Antoniadis, N. Arkani-Hamed, S. Dimopoulos, and G. Dvali, Phys. Lett. B **436**, 257 (1998).
[39] N. Arkani-Hamed, S. Dimopoulos, and G. Dvali, Phys. Lett. B **429**, 263 (1998).
[40] N. Arkani-Hamed, S. Dimopoulos, and G. Dvali, Phys. Rev. D **59**, 086004 (1999).
[41] L. Randall and R. Sundrum, Phys. Rev. Lett. **83**, 4690 (1999).
[42] L. Randall and R. Sundrum, Phys. Rev. Lett. **83**, 3370 (1999).
[43] A. Freitas and K. Kong, J. High Energy Phys. 02 (2008) 068.
[44] B. A. Dobrescu and E. Poppitz, Phys. Rev. Lett. **87**, 031801 (2001).
[45] G. Burdman, AIP Conf. Proc. **903**, 447 (2007).
[46] K. Ghosh and A. Datta, Nucl. Phys. **B800**, 109 (2008).
[47] T. Appelquist, B. A. Dobrescu, E. Ponton, and H.-U. Yee, Phys. Rev. Lett. **87**, 181802 (2001).
[48] B. A. Dobrescu, K. Kong, and R. Mahbubani, J. High Energy Phys. 07 (2007) 006.
[49] G. Burdman, B. A. Dobrescu, and E. Ponton, Phys. Rev. D **74**, 075008 (2006).
[50] A. Buras, M. Misiak, M. Mnz, and S. Pokorski, Nucl. Phys. **B424**, 374 (1994).
[51] M. Misiak, Nucl. Phys. **B393**, 23 (1993); **B439**, 461(E) (1995).
[52] B. Buras and M. Munz, Phys. Rev. D **52**, 186 (1995).

[53] R. S. Chivukula, D. A. Dicus, H.-J. He, and S. Nandi, Phys. Lett. B **562**, 109 (2003).
[54] J. Beringer *et al.* (Particle Data Group), Phys. Rev. D **86**, 010001 (2012).
[55] Y.-M. Wang, Y. Li, and C.-D. Lü, Eur. Phys. J. C **59**, 861 (2009).
[56] P. Colangelo, F. De Fazio, R. Ferrandes, and T. N. Pham, Phys. Rev. D **77**, 055019 (2008).
[57] C.-S. Huang and H.-G. Yan, Phys. Rev. D **59**, 114022 (1999); **61**, 039901(E) (2000).
[58] R. Mohanta, A. K. Giri, M. P. Khanna, M. Ishida, and S. Ishida, Prog. Theor. Phys. **102**, 645 (1999).
[59] L.-F. Gan, Y.-L. Liu, W.-B. Chen, and M.-Q. Huang, Commun. Theor. Phys. **58**, 872 (2012).
[60] T. Mannel and S. Recksiegel, J. Phys. G **24**, 979 (1998).
[61] P. Biancofiore, J. Phys. G **40**, 065006 (2013).